A Topological Model of the Interaction between α-Synuclein and Sodium Dodecyl Sulfate Micelles†

Marco Bisaglia,‡ Isabella Tessari,§ Luca Pinato,‡ Massimo Bellanda,‡ Sabrina Giraudo,|| Mauro Fasano,⊥ Elisabetta Bergantino,§ Luigi Bubacco,§ and Stefano Mammi*,‡

Department of Chemical Sciences, University of Padova, Via F. Marzolo 1, 35131 Padova, Italy, Department of Biology, University of Padova, Viale G. Colombo 3, 35121 Padova, Italy, Department of Neuroscience, University of Turin, Via Cherasco 15, 10126 Torino, Italy, and Department of Structural and Functional Biology, University of Insubria, Via Alberto da Giussano 12, 21052 Busto Arsizio, Italy

Received July 21, 2004; Revised Manuscript Received October 18, 2004

ABSTRACT: Human α-synuclein is a 140-amino acid protein of unknown function abundantly expressed in the brain and found in Lewy bodies, a characteristic feature of Parkinson's disease. α-Synuclein is random in water under physiological conditions, but the first ∼100 residues interact with SDS micelles or acidic phospholipid small unilamellar vesicles and adopt an ordered conformation. The rest of the molecule remains disordered in the bulk of the solution. The conformation of the N-terminal portion of the molecule in lipids was described as an extended helix [Ramakrishnan, M., Jensen, P. H., and Marsh, D. (2003) *Biochemistry 42*, 12919−12926], as two distinct α-helices interrupted by a two-residue break [Chandra, S., Chen, X., Rizo, J., Jahn, R., and Sudhof, T. C. (2003) *J. Biol. Chem*. *278*, 15313−15318], or as a noncanonical conformation, the α11/3 helix [Bussell, R., Jr., and Eliezer, D. (2003) *J. Mol. Biol*. *329*, 763−778]. We characterized the topology of the different regions of α-synuclein relative to the surface of SDS micelles using spin probe-induced broadening of NMR signals, ^{15}N relaxation measurements, and fluorescence spectroscopy. Our results support the presence of two N-terminal helices, positioned on the surface of the micelle and separated by a flexible stretch. The region of residues 61−95 of the protein also adopts a helical conformation, but it is partially embedded in the micelle. These results could shed some light on the role of the membrane on the aggregation process of α-synuclein.

Parkinson's disease (PD),[1] the second most common neurodegenerative disorder affecting 1−2% of the population over the age of 65 (*1*), is a chronic and progressive disease, caused by relentless degeneration of specific neuronal population in the brain, most notably the dopaminergic melanin-containing neurons of the substantia nigra pars compacta. Neuropathologically, it is characterized by the presence of Lewy bodies and dystrophic neurites (Lewy neurites), both comprised of cytoplasmic accumulations of aggregated proteins (*2*), specifically, α-synuclein and ubiquitin (*3*), which accompany the loss of dopaminergic neurons. The diffused occurrence of Lewy bodies is also observed in cortex tissues of patients affected by dementia with Lewy bodies, a severe cognitive impairment of sporadic origin (*4*).

Human α-synuclein is a 140-amino acid protein of unknown function that is abundantly expressed in the brain, where it is concentrated in presynaptic nerve terminals (*5*, *6*). The N-terminal region (approximately residues 1−95) of the α-synuclein sequence contains an imperfect 11-residue periodicity, with a highly conserved hexamer motif (KTKEGV), found in the A2 class of apolipoproteins and described as being potentially able to fold into an amphipathic α-helix (*7*). The peptide corresponding to residues 61−95, originally termed NAC (non-Aβ-amyloid component) was observed in amyloid plaques associated with Alzheimer's disease (*5*), although no association of α-synuclein as such with the mature plaques was detected (*8*). From a structural point of view, α-synuclein has a random conformation in water under physiological conditions (*9*−*11*). On the other hand, in the presence of sodium dodecyl sulfate (SDS) micelles or acidic phospholipid small unilamellar vesicles (SUV), the first ∼100 residues are able to associate with these membrane-like assemblies while the rest of the molecule remains in the bulk of the solution. The conformation of the N-terminal portion of the molecule in SDS was described as an extended helix (*9*), as two distinct α-helices interrupted by a two-residue break (*11*), or as a noncanonical

† This work was supported by a grant from the University of Padova (progetto di Ateneo 2002).

* To whom correspondence should be addressed. Phone: +39-0498275293. Fax: +39-0498275239. E-mail: stefano.mammi@unipd.it.

‡ Department of Chemical Sciences, University of Padova.

§ Department of Biology, University of Padova.

|| University of Turin.

⊥ University of Insubria.

[1] Abbreviations: CD, circular dichroism; DMPC, dimyristoylphosphatidylcholine; DMPG, dimyristoylphosphatidylglycerol; DPC, dodecylphosphocholine; DSA, doxylstearic acid; EPR, electron paramagnetic resonance spectroscopy; HSQC, heteronuclear single-quantum coherence; NAC, non-Aβ-amyloid component; NMR, nuclear magnetic resonance; NOESY, nuclear Overhauser effect spectroscopy; SDS, sodium dodecyl sulfate; SUV, small unilamellar vesicles; TOCSY, total correlation spectroscopy; PC, phosphatidylcholine; PD, Parkinson's disease; PS, phosphatidylserine; PE, phosphatidylethanolamine; PI, phosphatidylinositol.

10.1021/bi048448q CCC: $30.25
Published on Web 12/08/2004

conformation, the α11/3 helix (*12*). Two recent studies based on EPR measurements in SUV support the extended helix model (*13*, *14*).

The mechanisms responsible for Lewy body formation are not known. Three single-point mutations in α-synuclein, A30P, A53T, and E46K (*15*−*17*), as well as a triplication of the α-synuclein gene (*18*, *19*) have been linked to rare familial forms of Parkinson's disease, but the vast majority of Lewy body-related disease cases are sporadic and involve wild-type α-synuclein. *In vitro*, purified α-synuclein aggregates into fibrils resembling those found in Lewy bodies, following a nucleation pathway in which smaller oligomers are formed (*20*). Fibril assembly seems to occur through the repeats in the N-terminal half and to be accompanied by the transition from a random-coil conformation to a β-pleated sheet (*21*). In the fibrils found in the Lewy bodies, α-synuclein is indeed in a β-sheet structure.

Several pieces of evidence indicate that the NAC region of the protein is the most likely site for induction of β-sheet structure and consequent aggregation. This fragment is the second major component of amyloid plaques in Alzheimer's brain (*5*), and it was shown to readily adopt a β-sheet conformation at the highest concentrations that can be attained in a water solution (0.011 mM) (*22*). Another protein of the synuclein family, β-synuclein, is highly homologous to α-synuclein (*6*), but it does not form fibrils. The different behavior is most easily explained by the absence, in β-synuclein, of a stretch of hydrophobic residues in the central NAC region corresponding to residues 73−83 of α-synuclein (*23*, *24*). Finally, analysis of the N-terminal sequence of NAC revealed a degree of similarity to regions crucial for the aggregation and toxicity of three other amyloidogenic proteins, namely, Aβ, prion protein, and islet amyloid polypeptide. Specifically, a four-residue motif, G-A-X-X, where X represents an amino acid with an aliphatic side chain, is common to all four peptides (*25*).

The effect of lipids on the aggregation propensity of α-synuclein is more complex. Many articles appeared with results that are often contradictory. Membrane-bound α-synuclein has been suggested to play an important role in fibril formation (*26*), and the aggregation has been suggested to occur on membrane surfaces (*27*). In addition, the protein was demonstrated to be in a multimeric form when isolated from the membrane fraction of either brain or neuronal cell culture (*28*−*30*). However, some reports indicate that self-interaction of α-synuclein is suppressed by the presence of membranes in vitro (*31*) and that the α-helical conformation of the protein does not fibrillate (*32*, *33*).

In this study, we examined the topology of α-synuclein in a membrane-mimetic environment. Specifically, we characterized the position of the different regions of the protein relative to the micelles formed by SDS. The results of independent experimental approaches can be rationalized with the presence of two N-terminal α-helices positioned on the surface of the micelle and separated by a flexible stretch. The NAC region of the protein also adopts a helical conformation, but it is deeply embedded in the micelle. Sufficient experimental evidence is provided to suggest a topological model which describes the structuring effect of SDS micelles on α-synuclein. On these premises, an attempt is made to explain the role of the natural membrane on the aggregation process of α-synuclein.

EXPERIMENTAL PROCEDURES

Cloning and Expression of α-Synuclein 1−*140 (α-syn140) and α-Synuclein 1*−*99 (α-syn99).* Human α-synuclein cDNA, both the wild type and a deletion mutant (1−99), was subcloned into the pET-28b plasmid. Briefly, the coding regions were amplified via PCR using pMal-α-syn140 as a template, Taq DNA Polymerase (Promega), and synthetic oligonucleotides (Sigma-Genosys) containing restriction sites *Nde*I and *Xho*I. After digestion with restriction enzymes, the PCR products were inserted into the *Nde*I−*Xho*I-linearized pET-28b expression vector (Novagen), which contains a polyhistidine region followed by a thrombine cleavage site, and introduced into *Escherichia coli* strain BL21(DE3). Overexpression of proteins was achieved by growing cells in M9 minimal medium (supplemented with 1 g/L [^{15}N]-ammonium chloride for ^{15}N-labeled proteins) at 37 °C to an OD_{600} of ∼0.6 followed by induction with 0.5 mM isopropyl β-thiogalactopyranoside for 5 h. The proteins were purified on a Co−agarose TALON resin (Clontech), using the manufacturer's recommended protocol and stored in 20 mM phosphate buffer (pH 7.4). The purified proteins were digested with thrombin protease (Amersham Pharmacia) using the manufacturer's protocol. The final proteins contained an extra Gly-Ser-His sequence at the N-terminus.

Preparation of Small Unilamellar Vesicles. Approximately 8 mg of a mixture of 50% dimyristoylphosphatidylcholine and 50% dimyristoylphosphatidylglycerol were used for the preparation of SUV. The lipids were dissolved in 1 mL of a 4:1 chloroform/methanol mixture, and the solutions were evaporated under vacuum at 4 °C in a glass test tube. The dry lipid film was suspended in 100 mM sodium phosphate buffer (pH 7.4) to give a final concentration of 45 mM and mixed for 1 h above the melting temperature. The product of hydration was filtered through a large pore size (0.45 μm) filter and, subsequently, extruded through a 50 nm pore filter.

CD Experiments. CD measurements were carried out on a JASCO J-715 spectropolarimeter interfaced with a personal computer. The CD spectra were acquired and processed using the J-700 program for Windows. All experiments were carried out at room temperature using HELLMA quartz cells with Suprasil windows and an optical path length of 0.01 cm. All spectra were recorded in the wavelength range of 190−260 nm, using a bandwidth of 2 nm and a time constant of 2 s at a scan speed of 50 nm/min. The signal:noise ratio was improved by accumulating at least four scans. Spectra were acquired on 100 μM solutions of α-syn140 and α-syn99 in the presence of 50 mM phosphate buffer (pH 7.4) and with the addition of increasing amounts of dodecylphosphocholine (DPC) or SDS micelles, or SUV. All spectra are reported in terms of mean residue molar ellipticity $[\Theta]_R$ (degrees times square centimeters per decimole).

NMR Assignment. All NMR experiments were performed on a Bruker Avance DMX600 spectrometer equipped with a gradient triple-resonance probe. The spectra were processed using GIFA (*34*) and analyzed using XEASY (*35*) on a Silicon Graphics workstation. NMR samples used for the assignment of α-syn99 contained ∼2 mM protein in a H_2O/D_2O mixture (90:10, v/v), 20 mM phosphate buffer (pH 7.4), and 250 mM SDS-d_{25}. The experiments were performed at 25 °C.

Assignment of backbone NH groups and α-protons was initially based on that obtained by Chandra and co-workers (*11*) (BMRB accession number 5744) and then confirmed by means of three-dimensional (3D) TOCSY-HSQC experiments using a DIPSI2 isotropic mixing pulse sequence (*36*) and 3D NOESY-HSQC experiments with mixing times of 70 and 100 ms, respectively. The 3D experiments were acquired with 64 complex data points in the ^{15}N dimension, 200 or 150 in the ^{1}H indirect dimension and 1024 or 512 in the ^{1}H direct dimension. Spectral widths were 6009 or 2404 (^{1}H direct), 1338 (^{15}N), and 6000 Hz (^{1}H indirect). The frequency offsets were 2323.7 or 4800 (^{1}H direct), 7230 (^{15}N), and 2323.7 Hz (^{1}H indirect). A 90°-shifted sine function was used in the direct dimension, and a 90°-shifted sine^2 function was used in both indirect dimensions.

Paramagnetic Relaxation Experiments. The fHSQC sequence (*37*) was used for all NMR experiments and recorded at 25 °C in 20 mM phosphate buffer (pH 7.4) and 50 mM SDS-d_{25}. The protein concentration was 0.5 mM for both α-syn140 and α-syn99. Four series of paramagnetic relaxation experiments were acquired to investigate the topological orientation of α-synuclein in the presence of SDS micelles. 5-Doxylstearic acid (5-DSA) and 16-doxylstearic acid (16-DSA) (Aldrich) were dissolved in methanol-d_4 (CIL) to a concentration of 75 mM. Aliquots of these solutions were added to the NMR tube containing α-syn140 or α-syn99 and the SDS micelles for a final concentration of 0.5 mM of either spin probe (protein:spin probe ratio of 1). All recording parameters were kept rigorously constant, the only modification concerning the probe tuning and the field shimming. The experiments (512 increments of 512 time points each) were acquired with 32 transients each. The spectral widths were 2404 (^{1}H) and 1582 Hz (^{15}N) and the frequency offsets 4800 (^{1}H) and 7175 Hz (^{15}N). The spectra were identically processed to obtain 512 × 512 real points matrices. Prior to Fourier transformation, a 90°-shifted sine^2 function was used in both dimensions. Baseplane correction was applied before peak integration.

The NH amide peak intensities were measured before and after the addition of the paramagnetic probes and compared. The results are reported in terms of remaining amplitude (RA) defined by the equation RA = A(probe)/A(0), where A(probe) is the amplitude of the peak measured after the addition of the paramagnetic agent and A(0) is the amplitude in the absence of the paramagnetic agent. Uncertainties in peak intensity were determined by evaluating the noise level in a peak-free region of the spectra.

Relaxation Experiments. For the relaxation measurements, the same sample used for the assignment was utilized. The sensitivity-enhanced pulse schemes were used to measure relaxation rates R_1 and R_2 and the {^{1}H}−^{15}N NOEs (*38*). Each two-dimensional (2D) data set consisted of 512 real data points with a ^{1}H spectral width of 2404 Hz and 256 increments with a ^{15}N spectral width of 1582 Hz. Thirty-two scans were acquired for each increment; quadrature detection was achieved by using echo/antiecho-TPPI with gradient selection; the GARP broadband decoupling (*39*) scheme was applied to the ^{15}N spins during detection. The R_1 values were determined from 15 experiments using the following 10 relaxation delay times: 20 (twice), 70, 120, 200 (twice), 300, 500 (twice), 700, 950 (twice), 1200, and 1500 ms (twice). To determine R_2 relaxation rates, 15 spectra were recorded at 10 relaxation delay times: 8.8 (twice), 17.7 (twice), 26.5, 35.4 (twice), 44.2, 61.9, 79.6 (twice), 97.3, 123.9 (twice), and 159.3 ms. Duplicate spectra were collected at several delay times to estimate the uncertainties in measured peak intensities. The heteronuclear {^{1}H}−^{15}N NOEs were obtained by recording pairs of spectra in the presence and absence of ^{1}H saturation. Three pairs of experiments were carried out in an effort to evaluate the uncertainties in measuring the NOEs. For the R_1 and R_2 experiments, the recycle delay time was set to 2.2 s, while for {^{1}H}−^{15}N NOE measurements, the ^{1}H recovery period was set to 3.5 s. The time domain data were zero-filled to 1024 and 512 real data points in the F_2 and F_1 dimensions, respectively, in the spectra recorded for the determination of R_1 and to 2048 and 512 real data points, respectively, in the spectra recorded for the determination of R_2. In both cases, the spectra were apodized using a 90°-shifted sine^2 filtering function in both dimensions. Each spectrum was subjected to baseplane correction prior to integration. The relaxation rates were calculated using a least-squares fitting of peak heights versus relaxation delay by means of the Levenburg−Marquardt algorithm (*40*). The data were fitted using a three-parameter exponential model for the determination of R_1 and a two-parameter exponential model for R_2. Uncertainties in the fitted rates were estimated as described by Kordel et al. (*41*). Steady-state NOE values were calculated as the ratio of peak heights in the pair of spectra (with or without proton saturation). The variance of the pairwise ratios was used to estimate the experimental uncertainty.

The reduced spectral density mapping method (*42*) was applied to analyze the relaxation data. This approach makes no assumptions about the shape of the molecule or the nature of its motions.

Fluorescence Experiments. Fluorescence emission spectra were recorded on a Perkin-Elmer LS 50 spectrofluorimeter equipped with a thermostated cell compartment. The two synuclein samples of the 1−99 deletion mutant were obtained by dilution in 20 mM sodium phosphate buffer at pH 7.4 to obtain a final protein concentration of 100 μM, with or without 10 mM SDS. Protein solutions had an absorbance at the excitation wavelength (294 nm) of <0.05 to minimize the inner-filter or self-absorption effects. Spectra were recorded in the "ratio" mode to reduce the variations due to the fluctuation of the light source.

RESULTS

Effects of Phospholipid Vesicles and Detergents on α-Synuclein Secondary Structure. α-Synuclein has been reported to bind to acidic synthetic membranes such as PC/PS, PE/PS, PE/PA, and PE/PI membranes (*7*, *43*, *44*). Here, far-UV circular dichroism spectroscopy was used to determine the effects of small acidic unilamellar vesicles containing 50% phosphatidylcholine and 50% phosphatidylglycerol. As previously reported (*9*), our data indicate that lipid-free α-synuclein is unstructured in water under physiological conditions. The protein interacts with acidic SUV, undergoing a conformational transition to an α-helical state in a dose-dependent manner (Figure 1A). With increasing amounts of SUV, a progressive increase in the extent of α-synuclein folding was observed. The saturation value can be roughly

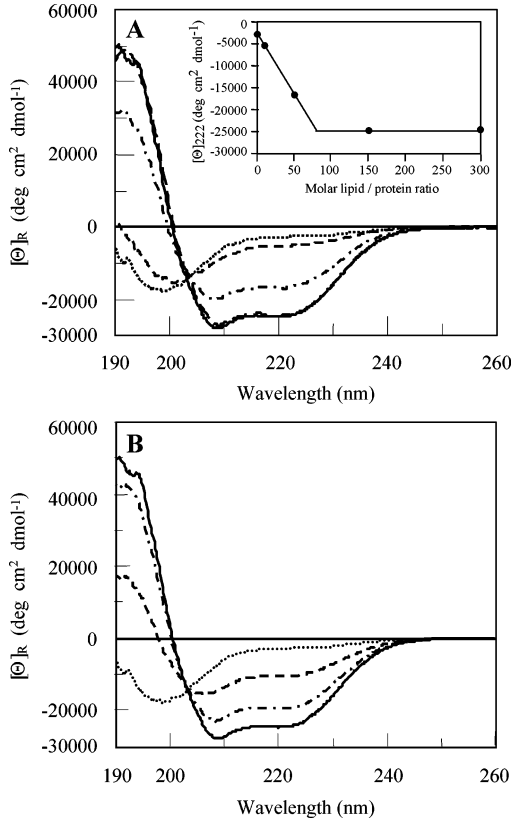

FIGURE 1: Phospholipid-induced folding of α-synuclein. (A) Far-UV CD spectra of α-synuclein (100 μM) as a function of the following 1:1 PC/PG SUV concentrations: 0, 1, 5, 15, and 30 mM. The inset represents the molar ellipticity of α-synuclein at 222 nm as a function of the lipid:protein molar ratio. (B) Far-UV CD spectra of α-synuclein in the presence of 20 mM phosphate buffer (pH 7.4) (•••) and with the addition of 10 mM DPC (- - -), 10 mM SDS (-•-), or 15 mM SUV (—). The concentrations of SDS or DPC are above their respective critical micellar concentrations, and the spectra remain identical with increasing amounts of detergent (data not shown).

extrapolated to a molar lipid:protein ratio of ~80 (inset of Figure 1A). This value is in agreement with that estimated by Ramakrishnan et al. (*13*) (ratio of ~100) using 100% DMPG vesicles, and it is smaller than the value found by Chandra et al. (*11*) (ratio of ~270−300), using 70:30 PC/PS SUV, indicating an effect of the composition and of the charge of the lipids on the α-helical propensity of α-synuclein. The presence of a well-defined isodichroic point indicates that the equilibrium is between only two conformational states, i.e., a random coil and an α-helical structure.

CD spectroscopy was also utilized to compare the structuring effects of SUV with those induced by SDS and DPC, which are able to form acidic and zwitterionic micelles, respectively, and are widely used as membrane-mimetic environments (*45*−*49*). Both SDS and DPC micelles interact with α-synuclein, but only the acidic ones induce a degree of α-helix quantitatively comparable to that of SUV (Figure 1B). Also, the HSQC spectrum of α-syn140 in DPC is much less disperse than in SDS and is indicative of a less ordered structure (data not shown). The CD properties of α-syn99 in the same systems were very similar to those of the wild-type protein (data not shown). On these bases, we decided to use SDS micelles as the membrane-mimetic environment for the NMR analysis. This system is more amenable than SUV to NMR studies and has been already utilized in two structural studies on α-synuclein (*11*, *12*) after Chandra et al. verified that the modes of binding to the protein and the folding in negatively charged SUV or SDS micelles were comparable (*11*).

Positioning Studies of α-Synuclein in Micelles. The topology of α-synuclein in a membrane-mimetic environment was investigated by NMR, using as structural probes the effects of two different spin-labeled stearates on the amide resonances in the assigned ^{1}H−^{15}N HSQC spectra. Specifically, 5-DSA and 16-DSA were used to induce selective broadening of resonances from residues located at different depths in the micelle. The position of the spin probes inside the micelle has been previously determined from ^{13}C NMR experiments (*50*). The nitroxide group of 5-DSA is localized close to the sulfate group of the micelle, while 16-DSA is found in a region at the center of the micelle that is not very well defined. To interpret the results from NMR experiments in a quantitative manner, the percent reduction of the intensity of each amide peak with spin probes relative to the peak without relaxing agents was measured. This method has been widely employed (*51*−*53*) and provides quick and reliable answers. The principal advantage of using the reduction of signal intensities instead of the line broadening is the much higher sensitivity.

The results obtained for α-syn140 are shown in panels A and B of Figure 2. In the presence of either 5-DSA or 16-DSA, remarkable reductions in the intensity of peaks were observed for residues in the 1−99 N-terminal region, whereas the peak intensities for the 40 C-terminal residues were affected only to a minimal extent by the addition of spin probes. These results clearly confirm previous results that the C-terminal portion of the protein, approximately the last 40 residues, is exposed to the solvent whereas the 1−99 N-terminal region interacts with the SDS micelles (*9*, *11*, *12*). However, because of the severe overlap of many peaks (only 56 residues were visible in the 1−99 region of the entire protein), a detailed, residue-by-residue analysis was not possible. To better characterize the NAC region of the protein, the same analysis was repeated on the 1−99 deletion mutant of α-synuclein. The HSQC spectrum obtained in this case was much simpler to analyze (see the Supporting Information), with reduced peak overlap (14 residues). The assignment was verified using three-dimensional ^{1}H−^{15}N TOCSY-HSQC and NOESY-HSQC experiments. As expected, significant differences from the assignment published by Chandra and co-workers for the entire α-synuclein (*11*) were not found except at the two termini of the sequence where the chemical environment differs from that of the wild-type protein.

The effects of paramagnetic agents on α-syn99 are depicted in panels C and D of Figure 2. In the presence of 5-DSA, the reduction in peak intensities is slightly more pronounced in the NAC region, suggesting that this portion of the protein penetrates more deeply into the micelle. The effects observed in the presence of 16-DSA are less pronounced for the 20 N-terminal residues. A certain periodicity is evident in the first part of the sequence, especially for the effect of 5-DSA. A Fourier analysis of the data was performed (see the Discussion). Interestingly, it appears that the reduction in peak intensities varies in a linear manner from residue 61 to 99, and it is more marked in the 81−99 region. Another aspect that stems from this

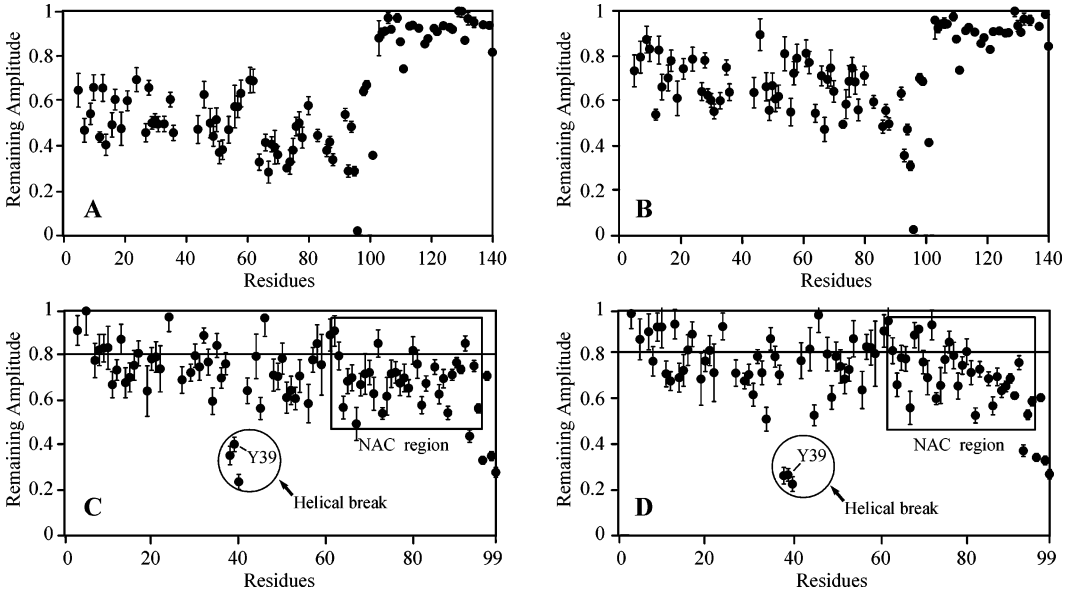

FIGURE 2: NMR studies of paramagnetic relaxation induced by nitroxide radicals on α-synuclein. (A and B) Remaining amplitude of the amide peaks of α-syn140 (500 μM) in the presence of 50 mM SDS after the addition of 500 μM 5-DSA (A) or 500 μM 16-DSA (B). (C and D) Remaining amplitude of the amide peaks of α-syn99 (500 μM) in the presence of 50 mM SDS after the addition of 500 μM 5-DSA (C) or 500 μM 16-DSA (D).

analysis is that the region around residue 40, previously shown to form a helical break (*11*), seems to penetrate into the micelle.

To define the localization of the Y39 residue with respect to the micelle, the fluorescence emission of this unique tyrosine (in the 1−99 deletion mutant) was quantified in the presence and absence of SDS. As previously observed in transmembrane synthetic peptides (*54*), the line shape of the emission spectra of tyrosine is not affected by the surrounding environment, but its intensity is. The addition of SDS to the α-syn99 sample produced a 20% increase in the intensity of the emission spectra as expected when the tyrosine shifts from a hydrophilic to a hydrophobic environment (data not shown).

Relaxation Parameter Analysis. To investigate the backbone dynamics of α-syn99 in SDS micelles, we measured its ^{15}N relaxation rates R_1 and R_2, as well as the $\{^1H\}-^{15}N$ NOE at a field strength of 14.1 T. These parameters are useful probes in analyzing the dynamics of proteins in various time scale ranges. All of them are influenced by motion on the pico- to nanosecond time scale, while T_2 can also reflect the contribution of motion on the micro- to millisecond time scale. Despite the relatively poor dispersion of the amide proton signals in the $^1H-^{15}N$ HSQC experiments used to measure the relaxation parameters, 85 of 99 residues could be used to characterize the backbone dynamics of α-syn99. Analysis of the 14 remaining amide groups was precluded due to signal overlap and a lack of assignment. The data for the identified residues are reported in Figure 3.

From the average R_2/R_1 ratio, the overall correlation time was estimated (*55*). Using only the 49 residues of α-syn99 satisfying the conditions described by Barbato et al. (*56*), a τ_C value of 11.4 ± 0.4 ns was found. This value corresponds to the correlation time expected for a globular protein of 20−25 kDa and is in good agreement with the value found by other authors for a small helical protein in SDS micelles (*57*). Considering that the molecular mass of α-syn99 is 10.2 kDa, it is possible to calculate that ∼40−50 molecules of

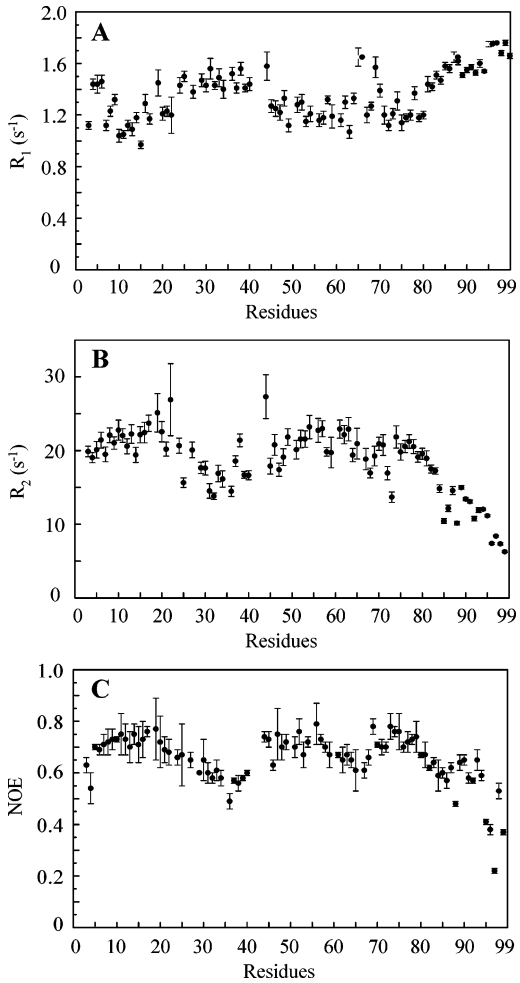

FIGURE 3: Plots of (A) R_1, (B) R_2, and (C) $\{^1H\}-^{15}N$ NOE relaxation data as a function of residue number. Data were acquired at 600 MHz on a sample of α-syn99 in the presence of SDS.

SDS are associated with the protein. A similar conclusion can be reached from theoretical considerations (*58*). The volume of the hydrophobic core of a micelle containing 40−

50 SDS molecules is $\sim 13-16 \times 10^3$ Å^3. The volume of the entire micelle can be calculated to be $23-32 \times 10^3$ Å^3, considering a hydrodynamic radius of an ideally spherical micelle 3−4 Å longer than that of the hydrophobic core. Since the average density of a protein is 1.33 g/cm^3 (*59*), the volume occupied by α-syn99 is $\sim 13 \times 10^3$ Å^3. The total volume of the micelle−protein assembly is therefore $36-45 \times 10^3$ Å^3. Using these values in the Stokes−Einstein equation together with our estimation of τ_C, one derives a viscosity for the solution of 1.0−1.4 cP, which is expected for a 250 mM solution of SDS (*60*, *61*).

In the slow motion regime, higher flexibility is revealed as increased R_1 and decreased R_2 relaxation rates as well as decreased heteronuclear $\{^1H\}-^{15}N$ NOE. From a global analysis of the three panels of Figure 3, it is possible to recognize four regions that clearly exhibit different relaxation behavior. These differences are particularly pronounced for the R_2 values and less evident in the case of R_1. The first region is the N-terminus, up to approximately residue 22. Here, the R_1 values are relatively low (average of ~ 1.22 s^{-1}) while the R_2 and the NOE average values (~ 21.7 s^{-1} and ~ 0.71, respectively) are significantly higher than those of the rest of the sequence. In the second region, between residues 24 and 44, the average value of R_1 increases to 1.46 s^{-1} while the values of both R_2 and NOE decrease (average values of 17.2 s^{-1} and 0.60, respectively). This indicates that this region is more flexible than the previous one. The third region comprises approximately residues 45−80. Here, the relaxation parameters are very similar to the ones measured for the N-terminal part of the protein. The last region includes the 19 C-terminal residues (81−99) and presents a rather different behavior compared with the rest of the protein. The gradual decrease in R_2 and NOE is clearly visible, while R_1 increases steadily. These features are consistent with a greater mobility of this portion of the backbone.

Reduced Spectral Density Mapping Approach. The relative amount of NH bond vector fluctuations at different frequencies was quantified using the reduced spectral density approach. This method allows one to obtain information about the motions of the polypeptide chain without making any assumption about the shape of the protein or about the time scale of the internal and global tumbling. The values of the spectral density function for each $^{15}N-^1H$ vector at three different frequencies were obtained in the approximation that this function does not vary in the interval from $\omega_H + \omega_N$ to $\omega_H - \omega_N$ (*42*). Figure 4 illustrates the reduced spectral density functions $J(0)$, $J(\omega_N)$, and $J(\omega_H+\omega_N)$ derived from relaxation parameters R_1 and R_2 and the $\{^1H\}-^{15}N$ NOE. These values reflect the contributions of the motion on the N−H vector on the different time scales: while the spectral density function at zero frequency, $J(0)$, is sensitive to motions on all time scales, the values of the spectral density functions at high frequencies, $J(\omega_N)$ and $J(\omega_H+\omega_N)$, are sensitive to fast internal motions on the $1/\omega_N$ and $1/\omega_H$ time scales.

Because the spectral density function is the Fourier transform of the reorientation correlation function, flexible residues with rapidly decaying correlations correspond to spectral density functions $J(\omega)$ decaying slowly toward higher values of ω. Therefore, $J(\omega_H+\omega_N)$ increases with an increase in flexibility, whereas $J(0)$ decreases.

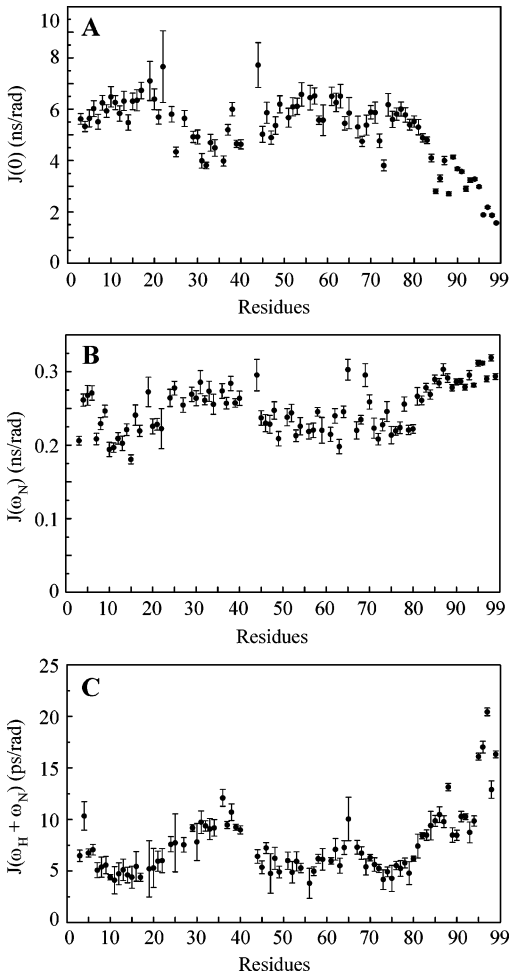

FIGURE 4: Reduced spectral density functions (A) $J(0)$, (B) $J(\omega_N)$, and (C) $J(\omega_H+\omega_N)$ as a function of residue number. Values were calculated from data depicted in Figure 3.

The behavior of the spectral density function parallels that of the raw experimental data. The $J(0)$ values are influenced mainly by the R_2 values, and this is reflected in the similarity of the two graphs. Conversely, $J(\omega_N)$ and $J(\omega_H+\omega_N)$ values are influenced by only R_1 and the NOE. Figure 4 underlines the clear appearance of four segments in the protein with different dynamical behavior. These zones correspond to the four identified in the analysis of the relaxation parameters. The first region (residues 1−22) and the third one (residues 44−80) are characterized by high $J(0)$ values and low $J(\omega_N)$ and $J(\omega_H+\omega_N)$ values. This behavior is typical of zones with restricted flexibility on fast time scales. The reduced flexibility of these regions of α-syn99 may be the consequence of a strong interaction between these amphipathic helical portions and the SDS micelles. On the other hand, residues 23−43, as well as the C-terminal part of the molecule, have relatively higher values of $J(\omega_N)$ and $J(\omega_H+\omega_N)$ and smaller values of $J(0)$, in line with a larger flexibility for these segments. The 20 C-terminal residues show a gradual decrease in $J(0)$ values toward the end of the chain. This effect is accompanied by the corresponding increase in the $J(\omega_H+\omega_N)$ values. This could indicate that the C-terminus is not anchored to the micellar surface as most of the residues are in the N-terminal part, but it is free to fluctuate.

It is worth noticing at this point that around residues 65 and 84 there are two short segments that are significantly

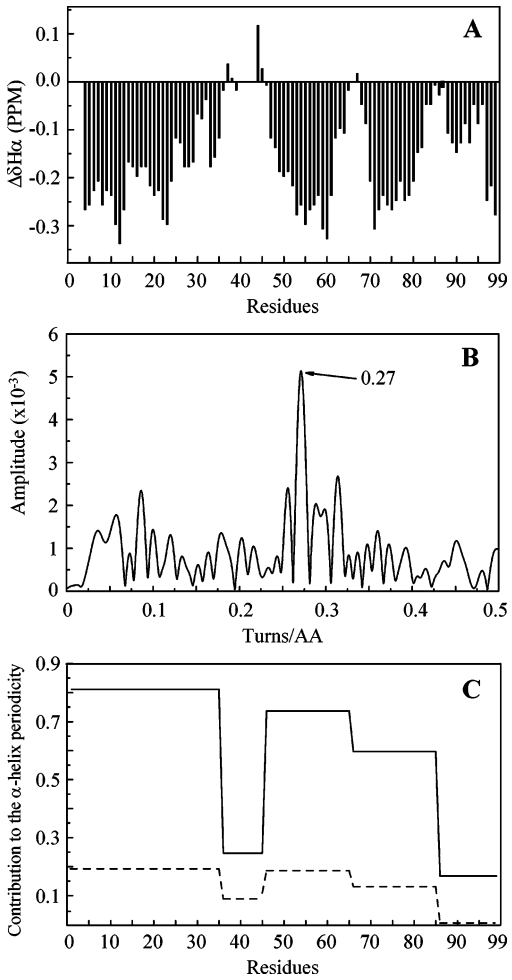

FIGURE 5: Analysis of secondary shifts of backbone amide and α-protons. (A) Plot of the H_α chemical shift deviations from a random coil conformation observed for α-syn99 in SDS as a function of residue number. Each data point was averaged with its nearest neighbors to eliminate local effects (*62*). Random coil chemical shifts were taken from ref *83*. (B) Fourier transform of the amide proton chemical shift deviations from a random coil conformation observed for α-syn99 in SDS (*84*) as a function of residue number. The data were zero-filled to 3000 data points before Fourier transformation to enhance resolution. (C) Frequency analysis of amide proton chemical shift deviations (—) and of the remaining amplitudes after the addition of 5-DSA (- - -). The Fourier transform was performed in various regions of the protein (residues 1−35, 1−45, 1−65, 1−85, and 1−99). The intensity of the peak at a frequency of 0.27 depends on the number of residues and on the contribution to the periodicity introduced by each of these residues. The contribution of different regions of the protein to the periodicity is reported. The contribution of residues 1−35 was evaluated by measuring the peak intensity, while for the other regions, the contributions were estimated from the differences in the intensity of the various regions: $I_{1-45} - I_{1-35} = I_{36-45}$; $I_{1-65} - I_{1-45} = I_{46-65}$; $I_{1-85} - I_{1-65} = I_{66-85}$; and $I_{1-99} - I_{1-85} = I_{86-99}$. The values were normalized by the number of residues in the region that was being considered.

more mobile than the surrounding regions (see the Discussion).

Chemical Shift Analysis. We analyzed the α-proton chemical shifts of α-syn99 to verify if the helical structure is present in the shorter construct (*62*−*64*). The results are shown in Figure 5A. Most of the protein shows a negative shift typical of a helical conformation, but three breaks are evident. The first one is approximately between residues 36 and 45, in a region of higher flexibility and comprising residues very strongly affected by 16-DSA. Two other shorter helical breaks are quite clear around residues 66 and 86, where an increased flexibility was estimated from the analysis of the reduced spectral densities.

It has been shown that the secondary shifts of the amide protons belonging to amphipathic helices have a periodicity of three to four residues (*65*−*67*). The Fourier transform of the amide proton secondary shifts of α-syn99 yields a peak at a frequency of 0.27, i.e., the expected value for the periodicity of the α-helix (Figure 5B). Different regions of the protein provide different contributions to the periodicity (Figure 5C). Specifically, insignificant contributions arise from residues 36−45, in agreement with the disruption of the α-helical structure, and from residues 85−99.

DISCUSSION

The recent demonstration that α-synuclein is the major component of the intracellular aggregates known as Lewy bodies, a central feature of Parkinson's disease, has spurred enormous interest in the study of this protein. The mechanisms that cause the change in conformation of α-synuclein and its assembly into fibrils are yet to be clarified; however, several lines of evidence indicate a critical role of the NAC region of the protein (*24*).

A key feature in the sequence of α-synuclein is the presence of seven imperfect 11-amino acid repeats in the first 93 residues with a highly conserved hexamer motif (KTKEGV), which are also features typical of the amphipathic α-helices of the apolipoproteins. In a previous work (*7*), the entire α-synuclein sequence was subjected to helical wheel analysis (*68*). By using the rules of Segrest et al. (*69*) that define several amphipathic α-helix-terminating amino acids, the authors identified five potential amphipathic α-helices which encompass all of the 11-mer repeats and some adjacent amino acid residues. The first four helices (residues 1−61) share the defining properties of class A2 lipid-binding helices, distinguished by clustered basic residues at the polar−apolar interface and positioned ±100° from the center of the apolar face. The predominance of basic residues over acidic ones and their position within the helix explain why α-synuclein interacts more strongly with acidic phospholipid vesicles. Different from the other ones, helix 5, comprising residues 62−95, is much more hydrophobic, with the presence of only one lysine in position 80 and one glutamic acid in position 83 as charged residues. These amino acids are located on the same face of the helix so that they can form a salt bridge leading to a neutral net charge.

All the topological models proposed so far suggest that α-synuclein binds only to lipid surfaces and does not insert into the interior of membranes. After the earliest model (*7*), the conformation of α-synuclein in membrane-mimetic environments such as acidic SUVs and SDS micelles was analyzed by NMR spectroscopy (*11*). On the basis of NOE restraints obtained for SDS-bound α-synuclein, N-terminal residues 1−98 were shown to possess an α-helical structure formed by two distinct α-helices interrupted by a two-residue break at positions 43 and 44, whereas the 42 C-terminal residues retain a random coil configuration. The presence of the break between the two helices was suggested to allow a more favorable binding of hydrophobic surfaces of the protein to the hydrophobic interior of the membrane-mimetic

milieu. Supposedly, both helices lie on the micellar surface. Another model, also based on NMR data, suggests the possibility that the 11-mer repeats of α-synuclein may lead to a noncanonical conformation, the α11/3 helix (*70*), for optimal hydrophobic interactions with the apolar lipid environment (*12*). Finally, two analyses of the lipid−protein interactions based on EPR methods indicate the presence of an extended helix encompassing the whole N-terminal region (*13*, *14*).

Our paramagnetic relaxation data clearly indicate that the N-terminal helix is not continuous. The Fourier analysis presented in Figure 5C shows a net discontinuity in the periodicity of the effect of 5-DSA around residue 40. Also, the chemical shift analysis supports the presence of a helical break in this position. Independently, ^{15}N relaxation measurements indicate two regions with reduced flexibility: residues 1−22 and residues 44−80. Conversely, residues 23−43 present a higher flexibility. This result can be explained by a strong interaction between the amphipathic helical portions and the SDS micelles. The particularly high value of R_2 observed for the residues in the amphipathic helices could be attributed to an additional motion, on a slow time scale (milliseconds to microseconds), between the flanking helical segments anchored on the micellar surface. In the calculation of τ_C, 17 residues were excluded on the basis of the slow motion criterion (*56*). Seven of these residues are comprised in the first helix and 10 in the second one. This motion is compatible with the fluctuations in size and shape of the micelles viewed as a fluid assembly.

The main break region (residues 36−45) contains a tyrosine at position 39. Recently, the importance of this tyrosine, along with Y125, for protein aggregation and cellular toxicity was underlined (*71*). The NMR-based models in the literature imply that Y39 is on the hydrophilic side of the helix (*11*, *12*) or possibly at the membrane−water interface (*12*). Also, Jao et al. (*14*) place Y39 on the hydrophilic face of their helix model, and suggest that the reduced dimensions and the higher curvature of the micelles relative to the phospholipid bilayers could introduce strain in the structure and produce a nonphysiological break in an otherwise elongated helix. Unfortunately, residue 39 was not mutated to Cys, and no specific data on this residue were collected (*14*). Also, the presence of immobilized components in the EPR spectra of proteins mutated at residues 35 and 41 is conspicuous, and its interpretation is not straightforward (*14*). The strong effect of both 5-DSA and 16-DSA on its amide resonance, supported by fluorescence measurements, strongly suggests that Y39 is inserted into the micelle. The *in vivo* implications of this possible arrangement are not easy to extrapolate, but it is possible that the membrane exerts a protective role toward α-synuclein aggregation by sequestering Y39 from the solvent. Unquestionably, this model explains why residue Y39 is not phosphorylated by p72^{syk} tyrosine kinase, whereas all the other tyrosyl residues, located in the C-terminal segment of the protein (Y125, Y133, and Y136), are (*72*).

No structural model anticipates the NAC region of the protein to form a transmembrane helix, despite its high hydrophobicity. However, predictions using the algorithm of von Heijne (*73*, *74*) or that of Hofmann and Stoffel (*75*) find a possible transmembrane segment between residues 62 and 82 or residues 63 and 95, respectively (data not shown). The higher mobility of the NAC region relative to that of the N-terminal portion and its higher sensitivity to micelle-bound spin probes lead to the conclusion that these residues are free to move in the interior of the micelle. It is surprising that the four C-terminal residues (Lys-Lys-Asp-Gln-OH) are among the most affected by 16-DSA, since they are charged. It is possible that these charges are neutralized through formation of internal salt bridges. An alternative explanation can be derived from the observation that the spin probes affect the protein *backbone* which can be a few angstroms from the charged side chain. As a consequence, it is possible that the charges are on the surface while the backbone is inside the micelle, in what is commonly termed "snorkeling" (*76*).

The apparent progressive immersion of residues 85−99 in the micelle is quite interesting. The frequency analysis performed both on the amide proton secondary shifts and on the effect of 5-DSA on α-syn99 supports the idea that this region does not form an amphipathic helix on the micellar surface since it does not contribute to the observed periodicity. It is enticing to extrapolate from these results and speculate that the NAC region could indeed be transmembrane *in vivo* and anchor the two extremities of the protein on opposite sites of the bilayer. It is clear that such conjecture needs to be backed up by experimental results. It is unfortunate that the thorough EPR analysis recently published did not probe the entire NAC region, but stopped at A90 (*14*). In that study, a consecutive scan of residues 59−90 led to the conclusion that a surface helix is present in this region. The center of the helix was estimated to be located at an immersion depth of 1−4 Å. This range is not in contrast with our data for two reasons: we observe clear embedding into the micelle for only residues beyond A90, and the periodicity detected by EPR is less pronounced between residues 80 and 90.

All the structural studies conducted on wild-type α-synuclein are in agreement with the idea that the central region of the protein, between residues 61 and 99, adopts a helical conformation. However, the lack of the last 40 C-terminal residues of the protein could disrupt this tendency, leading to a more disordered conformation of this region in α-syn99. We analyzed the α-proton chemical shifts of α-syn99 and verified that the helical structure is indeed present in the shorter construct. Similar conclusions were drawn by Bussell and Eliezer (*44*) on the basis of the α-carbon chemical shifts of their shorter constructs. With this method also, the presence of the same helical breaks detected by other techniques was identified. Bussell and Eliezer found that also the secondary C$^{\alpha}$ chemical shifts of the entire protein display discontinuity at several positions (*12*). Residues 43 and 44 were clearly identified as a helical break, while a diminished value at residues 65−68 and 83−86 was detected, although not as clearly as for the α-proton chemical shifts. While the N-terminal hinge might be useful in guaranteeing a better positioning of the amphipathic helical segments on the surface of the micelle, the latter two might introduce flexible points that allow the hydrophobic C-terminal helix to turn into the micelle. The C-terminal flexibility segment could also arise from local disruption of the helix brought about by the presence of the only charged residues in the NAC region, i.e., K80 and E83.

Critical comparison of these data and the literature structural data on α-synuclein underlines the question of the validity of SDS micelles as a membrane-mimetic environment for small proteins. As discussed above, the extreme curvature of the micelle could impose the helical break around position 40. The size of α-synuclein is comparable to that of a normal micelle, and an elongated α-helix would almost wrap completely around the micelle. The picture of α-synuclein interacting with a ball-shaped object is simplistic; the SDS could surround the protein in an asymmetric manner. It has been shown that a protein can alter the size and shape of the micelle (*48*, *49*). We also find that the presence of α-syn99 reduces the number of SDS molecules in the assembly to ∼50. Despite their drawbacks, micelles remain a reasonable choice for NMR structural and dynamic studies of biological macromolecules. Vesicles are more similar to the physiological environment, but their reorientation rates are too low for high-resolution NMR. With proper care, the information derived from studies in micelles can provide useful insights.

In this case, we chose SDS micelles which have been largely used in previous NMR studies of α-synuclein (*9*, *11*, *12*, *44*). As indicated above, the preference of α-synuclein for acidic micelles or vesicles may stem from a larger content of basic residues than acidic ones in the N-terminus. The effect of the surface charge has been recognized as a crucial determinant of α-synuclein−lipid interactions. On the basis of this observation, these authors propose a physiological role for α-synuclein in the context of synaptic vesicle biogenesis (*44*).

Our findings may shed some light on α-synuclein misfolding in relation to the purported pathogenic role of this protein in Parkinson's disease. Fibrillation has been proposed to occur via a nucleation-dependent mechanism (*77*) with the primary stage being the formation of a partially folded intermediate (*20*). These protofibrils, rather than fibrils themselves, may induce cell death (*78*, *79*). Accordingly, several studies indicate that α-synuclein protofibrils can modify the permeability of vesicles by formation of pores similar to those generated by pore-forming bacterial toxins (*79*−*81*). The altered membrane permeability could cause unregulated calcium flux and leakage of dopamine into the cytoplasm that leads to cell death (*79*). The NAC region of α-synuclein seems to be responsible for the ability of the protein to fibrillate (*24*). Our results indicate that this region is partially inserted in the micelle. A transmembrane disposition of the NAC region would exert a protective role against nucleation of aggregates and could explain why membrane-bound, α-helix-enriched α-synuclein does not fibrillate and cannot seed the fibrils (*31*−*33*), although lines of evidence to the opposite were also found (*26*, *27*).

Two different missense mutations in α-synuclein gene, resulting in the A53T and A30P substitutions, have been identified in a small number of kindreds with autosomal dominantly inherited, early onset PD (*15*, *16*). It has been demonstrated that these mutations accelerate the formation of protofibrils (*77*) and that the protofibrillar fraction comprising A53T and A30P had a greater specific pore forming activity (expressed as activity per mole of α-synuclein) than the wild type (*82*). Moreover, the observed decreased lipid affinity of A30P α-synuclein has been suggested to be responsible for the enhanced aggregation of this mutant (*44*). This hypothesis also can be explained by our model. As a consequence, the membrane-bound α-helical conformation of α-synuclein would be a nonpathological form of the protein, and this situation could be related to its physiological role.

ACKNOWLEDGMENT

We are grateful to Michele Scian for help with the analysis of the relaxation parameters.

SUPPORTING INFORMATION AVAILABLE

$^{1}H-^{15}N$ HSQC spectra of α-syn140 and α-syn99 in SDS micelles. This material is available free of charge via the Internet at http://pubs.acs.org.

REFERENCES

1. Lang, A. E., and Lozano, A. M. (1998) Parkinson's disease, *N. Engl. J. Med. 339*, 1130−1153.
2. Forno, L. (1996) Neuropathology of Parkinson's disease, *J. Neuropathol. Exp. Neurol. 55*, 259−272.
3. Spillantini, M. G., Schmidt, M. L., Lee, V. M., Trojanowski, J. Q., Jakes, R., and Goedert, M. (1997) α-Synuclein in Lewy bodies, *Nature 388*, 839−840.
4. Camicioli, R., and Fisher, N. (2004) Progress in clinical neurosciences: Parkinson's disease with dementia and dementia with Lewy bodies, *Can. J. Neurol. Sci. 31*, 7−21.
5. Ueda, K., Fukushima, H., Masliah, E., Xia, Y., Iwai, A., Yoshimoto, M., Otero, D. A., Kondo, J., Ihara, Y., and Saitoh, T. (1993) Molecular cloning of cDNA encoding an unrecognized component of amyloid in Alzheimer disease, *Proc. Natl. Acad. Sci. U.S.A. 90*, 11282−11286.
6. Jakes, R., Spillantini, M. G., and Goedert, M. (1994) Identification of two distinct synucleins from human brain, *FEBS Lett. 345*, 27−32.
7. Davidson, W. S., Jonas, A., Clayton, D. F., and George, J. M. (1998) Stabilization of α-synuclein secondary structure upon binding to synthetic membranes, *J. Biol. Chem. 273*, 9443−9449.
8. Wirths, O., and Bayer, T. A. (2003) α-Synuclein, Aβ and Alzheimer's disease, *Prog. Neuropsychopharmacol. Biol. Psychiatry 27*, 103−108.
9. Eliezer, D., Kutluay, E., Bussell, R., Jr., and Browne, G. (2001) Conformational properties of α-synuclein in its free and lipid-associated states, *J. Mol. Biol. 307*, 1061−1073.
10. Bussell, R., Jr., and Eliezer, D. (2001) Residual structure and dynamics in Parkinson's disease-associated mutants of α-synuclein, *J. Biol. Chem. 276*, 45996−46003.
11. Chandra, S., Chen, X., Rizo, J., Jahn, R., and Sudhof, T. C. (2003) A broken α-helix in folded α-synuclein, *J. Biol. Chem. 278*, 15313−15318.
12. Bussell, R., Jr., and Eliezer, D. (2003) A structural and functional role for 11-mer repeats in α-synuclein and other exchangeable lipid binding proteins, *J. Mol. Biol. 329*, 763−778.
13. Ramakrishnan, M., Jensen, P. H., and Marsh, D. (2003) α-Synuclein association with phosphatidylglycerol probed by lipid spin labels, *Biochemistry 42*, 12919−12926.
14. Jao, C. C., Der-Sarkissian, A., Chen, J., and Langen, R. (2004) Structure of membrane-bound α-synuclein studied by site-directed spin labeling, *Proc. Natl. Acad. Sci. U.S.A. 101*, 8331−8336.
15. Polymeropoulos, M. H., Lavedan, C., Leroy, E., Ide, S. E., Dehejia, A., Dutra, A., Pike, B., Root, H., Rubenstein, J., Boyer, R., Stenroos, E. S., Chandrasekharappa, S., Athanassiadou, A., Papapetropoulos, T., Johnson, W. G., Lazzarini, A. M., Duvoisin, R. C., Di Iorio, G., Golbe, L. I., and Nussbaum, R. L. (1997) Mutation in the α-synuclein gene identified in families with Parkinson's disease, *Science 276*, 2045−2047.
16. Kruger, R., Kuhn, W., Muller, T., Woitalla, D., Graeber, M., Kosel, S., Przuntek, H., Epplen, J. T., Schols, L., and Riess, O. (1998) Ala30Pro mutation in the gene encoding α-synuclein in Parkinson's disease, *Nat. Genet. 18*, 106−108.
17. Zarranz, J. J., Alegre, J., Gomez-Esteban, J. C., Lezcano, E., Ros, R., Ampuero, I., Vidal, L., Hoenicka, J., Rodriguez, O., Atares, B., Llorens, V., Gomez Tortosa, E., del Ser, T., Munoz, D. G., and de Yebenes, J. G. (2004) The new mutation, E46K, of

α-synuclein causes Parkinson and Lewy body dementia, *Ann. Neurol. 55*, 164−173.
18. Singleton, A. B., Farrer, M., Johnson, J., Singleton, A., Hague, S., Kachergus, J., Hulihan, M., Peuralinna, T., Dutra, A., Nussbaum, R., Lincoln, S., Crawley, A., Hanson, M., Maraganore, D., Adler, C., Cookson, M. R., Muenter, M., Baptista, M., Miller, D., Blancato, J., Hardy, J., and Gwinn-Hardy, K. (2003) α-Synuclein locus triplication causes Parkinson's disease, *Science 302*, 841.
19. Farrer, M., Kachergus, J., Forno, L., Lincoln, S., Wang, D. S., Hulihan, M., Maraganore, D., Gwinn-Hardy, K., Wszolek, Z., Dickson, D., and Langston, J. W. (2004) Comparison of kindreds with parkinsonism and α-synuclein genomic multiplications, *Ann. Neurol. 55*, 174−179.
20. Uversky, V. N., Li, J., and Fink, A. L. (2001) Evidence for a partially folded intermediate in α-synuclein fibril formation, *J. Biol. Chem. 276*, 10737−10744.
21. Serpell, L. C., Berriman, J., Jakes, R., Goedert, M., and Crowther, R. A. (2000) Fiber diffraction of synthetic α-synuclein filaments shows amyloid-like cross-β conformation, *Proc. Natl. Acad. Sci. U.S.A. 97*, 4897−4902.
22. Weinreb, P. H., Zhen, W., Poon, A. W., Conway, K. A., and Lansbury, P. T., Jr. (1996) NACP, a protein implicated in Alzheimer's disease and learning, is natively unfolded, *Biochemistry 35*, 13709−13715.
23. Giasson, B. I., Murray, I. V., Trojanowski, J. Q., and Lee, V. M. (2001) A hydrophobic stretch of 12 amino acid residues in the middle of α-synuclein is essential for filament assembly, *J. Biol. Chem. 276*, 2380−2386.
24. Uversky, V. N., and Fink, A. L. (2002) Amino acid determinants of α-synuclein aggregation: Putting together pieces of the puzzle, *FEBS Lett. 522*, 9−13.
25. El-Agnaf, O. M., and Irvine, G. B. (2000) Formation and properties of amyloid-like fibrils derived from α-synuclein and related proteins, *J. Struct. Biol. 130*, 300−309.
26. Lee, E. N., Lee, S. Y., Lee, D., Kim, J., and Paik, S. R. (2003) Lipid interaction of α-synuclein during the metal-catalyzed oxidation in the presence of Cu^{2+} and H_2O_2, *J. Neurochem. 84*, 1128−1142.
27. Cole, N. B., Murphy, D. D., Grider, T., Rueter, S., Brasaemle, D., and Nussbaum, R. L. (2002) Lipid droplet binding and oligomerization properties of the Parkinson's disease protein α-synuclein, *J. Biol. Chem. 277*, 6344−6352.
28. Lee, H. J., Choi, C., and Lee, S. J. (2002) Membrane-bound α-synuclein has a high aggregation propensity and the ability to seed the aggregation of the cytosolic form, *J. Biol. Chem. 277*, 671−678.
29. Leng, Y., Chase, T. N., and Bennett, M. C. (2001) Muscarinic receptor stimulation induces translocation of an α-synuclein oligomer from plasma membrane to a light vesicle fraction in cytoplasm, *J. Biol. Chem. 276*, 28212−28218.
30. Sharon, R., Goldberg, M. S., Bar-Josef, I., Betensky, R. A., Shen, J., and Selkoe, D. J. (2001) α-Synuclein occurs in lipid-rich high molecular weight complexes, binds fatty acids, and shows homology to the fatty acid-binding proteins, *Proc. Natl. Acad. Sci. U.S.A. 98*, 9110−9115.
31. Narayanan, V., and Scarlata, S. (2001) Membrane binding and self-association of α-synucleins, *Biochemistry 40*, 9927−9934.
32. Munishkina, L. A., Phelan, C., Uversky, V. N., and Fink, A. L. (2003) Conformational behavior and aggregation of α-synuclein in organic solvents: Modeling the effects of membranes, *Biochemistry 42*, 2720−2730.
33. Zhu, M., and Fink, A. L. (2003) Lipid binding inhibits α-synuclein fibril formation, *J. Biol. Chem. 278*, 16873−16877.
34. Pons, J. L., Malliavin, T. E., and Delsuc, M. (1996) Gifa version 4: A complete package for NMR data set processing, *J. Biomol. NMR 8*, 445−452.
35. Bartels, C., Xia, T. H., Billeter, M., Guntert, P., and Wüthrich, K. (1995) The program XEASY for computer-supported NMR spectral analysis of biological macromolecules, *J. Biomol. NMR 6*, 1−10.
36. Shaka, A. J., Lee, C. J., and Pines, A. (1988) Iterative schemes for bilinear operators; application to spin decoupling, *J. Magn. Reson. 77*, 274.
37. Mori, S., Abeygunawardana, C., Johnson, M. O., and Vanzijl, P. C. M. (1995) Improved sensitivity of HSQC spectra of exchanging protons at short interscan delays using a new fast HSQC (FHSQC) detection scheme that avoids water saturation, *J. Magn. Reson., Ser. B 108*, 94−98.
38. Skelton, N. J., Palmer, A. G. I., Akke, M., Kordel, I. J., Rance, M., and Chazin, W. J. (1993) Practical aspects of two-dimensional proton-detected ^{15}N spin relaxation measurements, *J. Magn. Reson., Ser. B 102*, 253−264.
39. Shaka, A. J., Barker, P. B., and Freeman, R. (1985) Iterative schemes for bilinear operators; application to spin decoupling, *J. Magn. Reson. 64*, 547−552.
40. Bevington, P. R. (1969) *Data Reduction and Error Analysis for the Physical Sciences*, McGraw-Hill, New York.
41. Kordel, J., Skelton, N. J., Akke, M., Palmer, A. G., III, and Chazin, W. J. (1992) Backbone dynamics of calcium-loaded calbindin D9k studied by two-dimensional proton-detected nitrogen-15 NMR spectroscopy, *Biochemistry 31*, 4856−4866.
42. Lefevre, J. F., Dayie, K. T., Peng, J. W., and Wagner, G. (1996) Internal mobility in the partially folded DNA binding and dimerization domains of GAL4: NMR analysis of the N−H spectral density functions, *Biochemistry 35*, 2674−2686.
43. Jo, E., McLaurin, J., Yip, C. M., St George-Hyslop, P., and Fraser, P. E. (2000) α-Synuclein membrane interactions and lipid specificity, *J. Biol. Chem. 275*, 34328−34334.
44. Bussell, R., Jr., and Eliezer, D. (2004) Effects of Parkinson's disease-linked mutations on the structure of lipid-associated α-synuclein, *Biochemistry 43*, 4810−4818.
45. Li, S. C., Goto, N. K., Williams, K. A., and Deber, C. M. (1996) α-Helical, but not β-sheet, propensity of proline is determined by peptide environment, *Proc. Natl. Acad. Sci. U.S.A. 93*, 6676−6681.
46. Melnyk, R. A., Partridge, A. W., and Deber, C. M. (2002) Transmembrane domain mediated self-assembly of major coat protein subunits from Ff bacteriophage, *J. Mol. Biol. 315*, 63−72.
47. Wang, G., Keifer, P. A., and Peterkofsky, A. (2003) Solution structure of the N-terminal amphitropic domain of *Escherichia coli* glucose-specific enzyme IIA in membrane-mimetic micelles, *Protein Sci. 12*, 1087−1096.
48. Vinogradova, O., Sönnichsen, F., and Sanders, C. R., II (1998) On choosing a detergent for solution NMR studies of membrane proteins, *J. Biomol. NMR 4*, 381−386.
49. Sanders, C. R., and Oxenoid, K. (2000) Customizing model membranes and samples for NMR spectroscopic studies of complex membrane proteins, *Biochim. Biophys. Acta 1508*, 129−145.
50. Papavoine, C. H., Konings, R. N., Hilbers, C. W., and van de Ven, F. J. (1994) Location of M13 coat protein in sodium dodecyl sulfate micelles as determined by NMR, *Biochemistry 33*, 12990−12997.
51. Chapin, V., Leenhouts, J., de Kroon, A., and de Kruijff, B. (1996) Secondary structure and topology of a mitochondrial presequence peptide associated with negatively charged micelles. A 2D ^1H NMR study, *Biochemistry 35*, 3141−3146.
52. Piserchio, A., Bisello, A., Rosenblatt, M., Chorev, M., and Mierke, D. F. (2000) Characterization of parathyroid hormone/receptor interactions: Structure of the first extracellular loop, *Biochemistry 39*, 8153−8160.
53. Monticelli, L., Pedini, D., Schievano, E., Mammi, S., and Peggion, E. (2002) Interaction of bombolitin II with a membrane-mimetic environment: An NMR and molecular dynamics simulation approach, *Biophys. Chem. 101−102*, 577−591.
54. Zhang, H., Bhargava, K., Keszler, A., Feix, J., Hogg, N., Joseph, J., and Kalyanaraman, B. (2003) Transmembrane nitration of hydrophobic tyrosyl peptides. Localization, characterization, mechanism of nitration, and biological implications, *J. Biol. Chem. 278*, 8969−8978.
55. Kay, L. E., Torchia, D. A., and Bax, A. (1989) Backbone dynamics of proteins as studied by ^{15}N inverse detected heteronuclear NMR spectroscopy: Application to staphylococcal nuclease, *Biochemistry 28*, 8972−8979.
56. Barbato, G., Ikura, M., Kay, L., Pastor, R. W., and Bax, A. (1992) Backbone dynamics of calmodulin studied by ^{15}N relaxation using inverse detected two-dimensional NMR spectroscopy: The central helix is flexible, *Biochemistry 31*, 5269−5278.
57. Papavoine, C. H. M., Remerowski, M. L., Horstink, L. M., Konings, R. N. H., Hilbers, C. W., and van de Ven, F. J. M. (1997) Backbone dynamics of the major coat protein of bacteriophage M13 in detergent micelles by ^{15}N nuclear magnetic resonance relaxation measurements using the model-free approach and reduced spectral density mapping, *Biochemistry 36*, 4015−4026.
58. Tanford, C. (1974) Theory of micelle formation in aqueous solution, *J. Phys. Chem. 78*, 2469−2479.

59. Squire, P. G., and Himmel, M. E. (1979) Hydrodynamics and protein hydration, *Arch. Biochem. Biophys. 196*, 165−177.
60. Akbas, H., Sidim, T., and Iscan, M. (2003) Effect of polyoxyethylene chain length and electrolyte on the viscosity of mixed micelles, *Turk. J. Chem. 27*, 357−363.
61. Trembleau, L., and Rebek, J., Jr. (2004) Interactions between a surfactant and cavitand in water blur distinctions between host and guest, *Chem. Commun.*, 58−59.
62. Pastore, A., and Saudek, V. (1990) The relationship between chemical shift and secondary structure in proteins, *J. Magn. Reson. 90*, 165−176.
63. Wishart, D. S., Sykes, B. D., and Richard, F. M. (1991) Relationship between nuclear magnetic resonance chemical shift and protein secondary structure, *J. Mol. Biol. 222*, 311−333.
64. Wishart, D. S., Sykes, B. D., and Richard, F. M. (1992) The chemical shift index: A fast and simple method for the assignment of protein secondary structure through NMR spectroscopy, *Biochemistry 31*, 1647−1651.
65. Kuntz, I. D., Kosen, P. A., and Craig, E. C. (1991) Amide chemical shift in many helices in peptides and proteins are periodic, *J. Am. Chem. Soc. 113*, 1406−1408.
66. Zhou, N. E., Zhu, B. Y., Sykes, B. D., and Hodges, R. S. (1992) Relationship between amide proton chemical shifts and hydrogen bonding in amphipathic α-helical peptides, *J. Am. Chem. Soc. 114*, 4320−4326.
67. Raussens, V., Slupsky, C. M., Sykes, B. D., and Ryan, R. O. (2003) Lipid bound structure of an apolipoprotein E-derived peptide, *J. Biol. Chem. 278*, 25998−26006.
68. Schiffer, J., and Edmundson, A. B. (1967) Use of helical wheels to represent the structures of proteins and to identify segments with helical potential, *Biophys. J. 7*, 121−135.
69. Segrest, J. P., Jones, M. K., De Loof, H., Brouillette, C. G., Venkatachalapathi, Y. V., and Anantharamaiah, G. M. (1992) The amphipathic helix in the exchangeable apolipoproteins: A review of secondary structure and function, *J. Lipid Res. 33*, 141−166.
70. Segrest, J. P., Jones, M. K., Klon, A. E., Sheldahl, C. J., Hellinger, M., De Loof, H., and Harvey, S. C. (1999) A detailed molecular belt model for apolipoprotein A-I in discoidal high-density lipoprotein, *J. Biol. Chem. 274*, 31755−31758.
71. Zhou, W., and Freed, C. R. (2004) Tyrosine-to-cysteine modification of human α-synuclein enhances protein aggregation and cellular toxicity, *J. Biol. Chem. 279*, 10128−10135.
72. Negro, A., Brunati, A. M., Donella-Deana, A., Massimino, M. L., and Pinna, L. A. (2002) Multiple phosphorylation of α-synuclein by protein tyrosine kinase Syk prevents eosin-induced aggregation, *FASEB J. 16*, 210−212.
73. von Heijne, G. (1992) Membrane protein structure prediction, hydrophobicity analysis and the positive-inside rule, *J. Mol. Biol. 225*, 487−494.
74. von Heijne, G. (1986) Mitochondrial targeting sequences may form amphiphilic helices, *EMBO J. 5*, 1335−1342.
75. Hofmann, K., and Stoffel, W. (1993) TMbase: A database of membrane spanning proteins segments, *Biol. Chem. Hoppe-Seyler 374*, 166.
76. Segrest, J. P., Deloof, H., Dohlman, J. G., Brouillette, C. G., and Anantharamaiah, G. M. (1990) Amphipathic helix motif: Classes and properties, *Proteins: Struct., Funct., Genet. 8*, 103−117.
77. Conway, K. A., Lee, S. J., Rochet, J. C., Ding, T. T., Williamson, R. E., and Lansbury, P. T., Jr. (2000) Acceleration of oligomerization, not fibrillization, is a shared property of both α-synuclein mutations linked to early-onset Parkinson's disease: Implications for pathogenesis and therapy, *Proc. Natl. Acad. Sci. U.S.A. 97*, 571−576.
78. Conway, K. A., Rochet, J. C., Bieganski, R. M., and Lansbury, P. T., Jr. (2001) Kinetic stabilization of the α-synuclein protofibril by a dopamine-α-synuclein adduct, *Science 294*, 1346−1349.
79. Volles, M. J., Lee, S. J., Rochet, J. C., Shtilerman, M. D., Ding, T. T., Kessler, J. C., and Lansbury, P. T., Jr. (2001) Vesicle permeabilization by protofibrillar α-synuclein: Implications for the pathogenesis and treatment of Parkinson's disease, *Biochemistry 40*, 7812−7819.
80. Volles, M. J., and Lansbury, P. T., Jr. (2002) Vesicle permeabilization by protofibrillar α-synuclein is sensitive to Parkinson's disease-linked mutations and occurs by a pore-like mechanism, *Biochemistry 41*, 4595−4602.
81. Lashuel, H. A., Hartley, D., Petre, B. M., Walz, T., and Lansbury, P. T., Jr. (2002) Neurodegenerative disease: Amyloid pores from pathogenic mutations, *Nature 418*, 291.
82. Volles, M. J., and Lansbury, P. T., Jr. (2003) Zeroing in on the pathogenic form of α-synuclein and its mechanism of neurotoxicity in Parkinson's disease, *Biochemistry 42*, 7871−7878.
83. Wishart, D. S., Sykes, B. D., and Richards, F. M. (1992) The chemical shift index: A fast and simple method for the assignment of protein secondary structure through NMR spectroscopy, *Biochemistry 31*, 1647−1651.
84. Wishart, D. S., Sykes, B. D., and Richards, F. M. (1991) Relationship between nuclear magnetic resonance chemical shift and protein secondary structure, *J. Mol. Biol. 222*, 311−333.

BI048448Q